

Supplementary materials

Biowaste valorization: multifunctional hybrid Lignin/TiO₂ nanostructures for bacterial-biocide disinfection and dye removal.

Marica Gallo ^a, Virginia Venezia ^{a,b*}, Marica Muscetta ^{a*}, Rossella Grappa ^a, Mariavittoria Verrillo ^c, Gianluca Landi ^d, Raffaele Marotta ^a, and Giuseppina Luciani ^a

^a DICMaPI, Department of Chemical, Materials and Industrial Production Engineering,
University of Naples Federico II, Naples, Italy

^b DiSt, Department of Structures for Engineering and Architecture, University of Naples
Federico II, Naples, Italy

^c Department of Agricultural Science, University of Naples Federico II, Portici, Italy

^d Institute of Sciences and Technologies for Sustainable Energy and Mobility-CNR, Naples,
Italy

Corresponding authors: virginia.venezia@unina.it; marica.muscetta@unina.it

Summary

1. Photocatalytic activity

Figure S-1

2. Results and Discussion

2.1 Physico-chemical characterization of hybrid TiO₂_DL nanoparticles

Table S-1

Figure S-2

Figure S-3

Figure S-4

Table S-2

Figure S-5

Figure S-6

Table S-3

Figure S-7

Figure S-8

2.2 Functional characterization of hybrid nanoparticles

Figure S-9

Figure S-10

Figure S-11

2.3 Antimicrobial and the antifungal characterization of hybrid nanoparticles

Figure S-12

3. Organic dyes removal: adsorption and photocatalytic degradation

Figure S-13

Figure S-14

Figure S-15

Figure S-16

Figure S-17

S.1. Experimental Setup

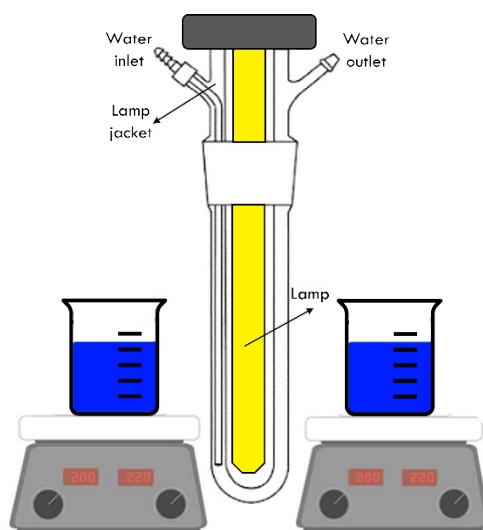


Figure S-1. Schematic illustration of the experimental set-up used for the photodegradation experiments.

S.2. Materials characterization

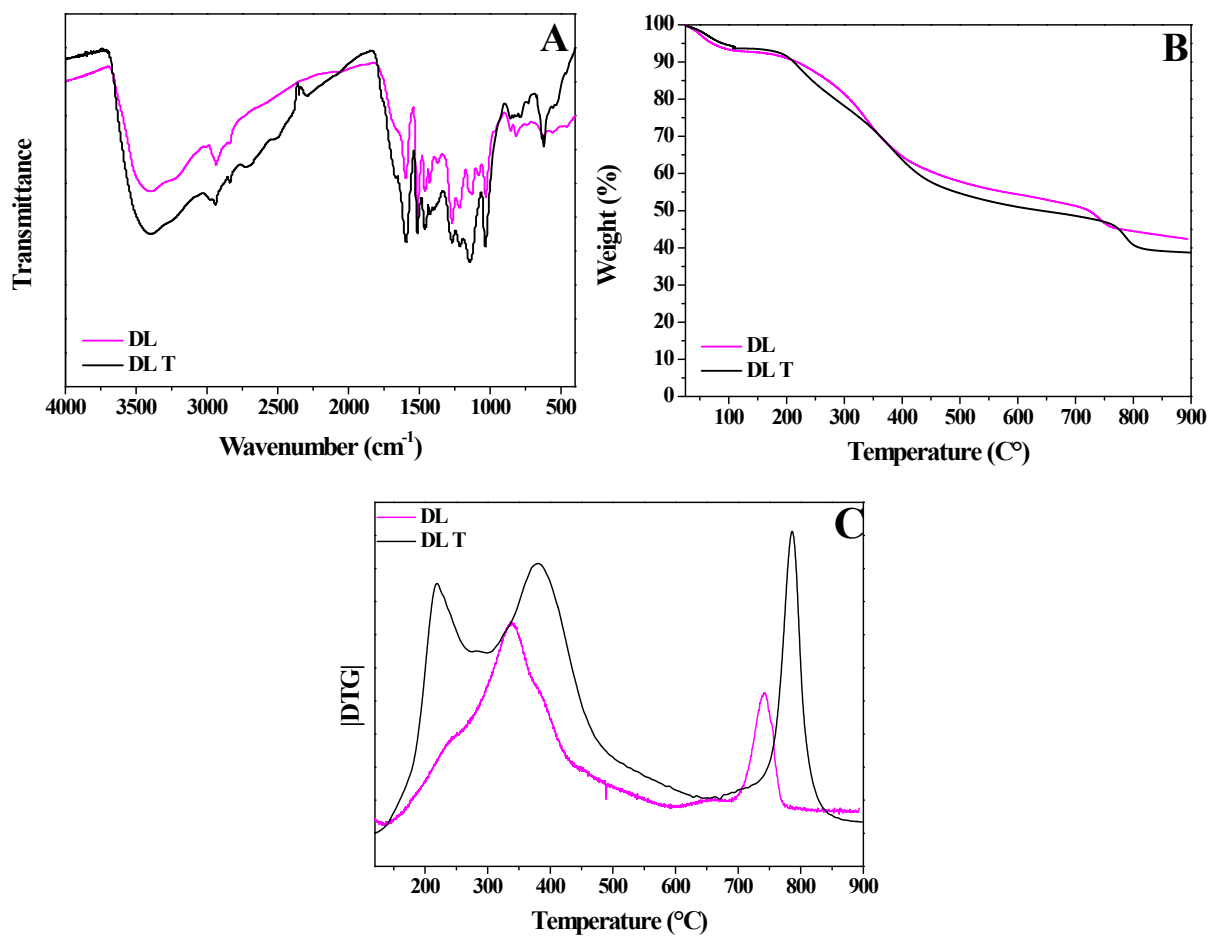


Figure S-2. FT-IR curves of DL and DL T (Panel A); TGA curves of DL and DL T samples (Panel B); DTG curves of DL and DL T samples (Panel C).

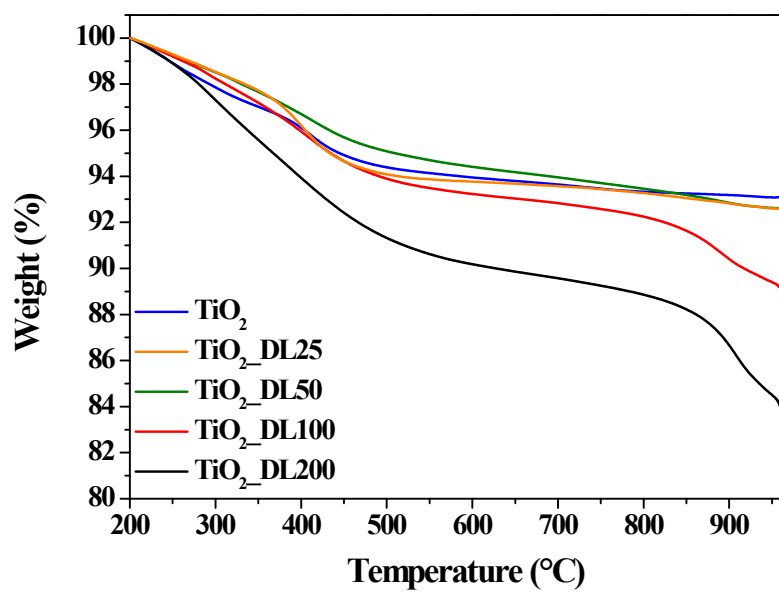


Figure S-3. TGA Curves of Bare TiO₂ and hybrid nanoparticles.

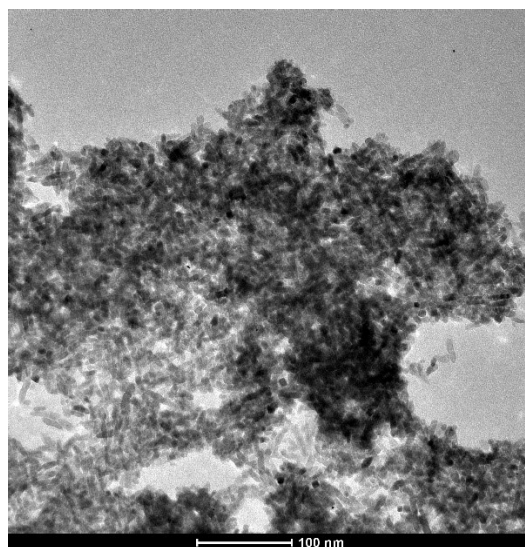


Figure S-4. TEM Micrograph of TiO₂ nanoparticles.

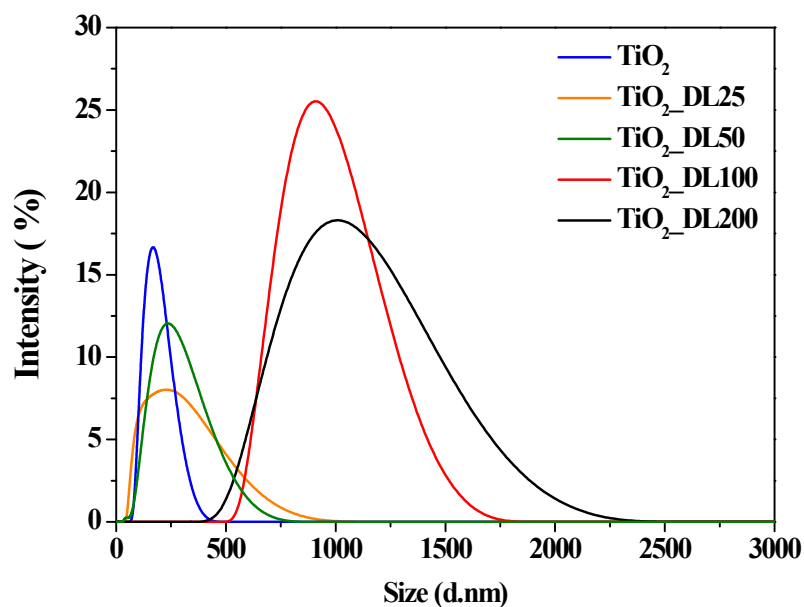


Figure S-5: Size distribution of bare TiO₂ and hybrid TiO₂_DL nanoparticles.

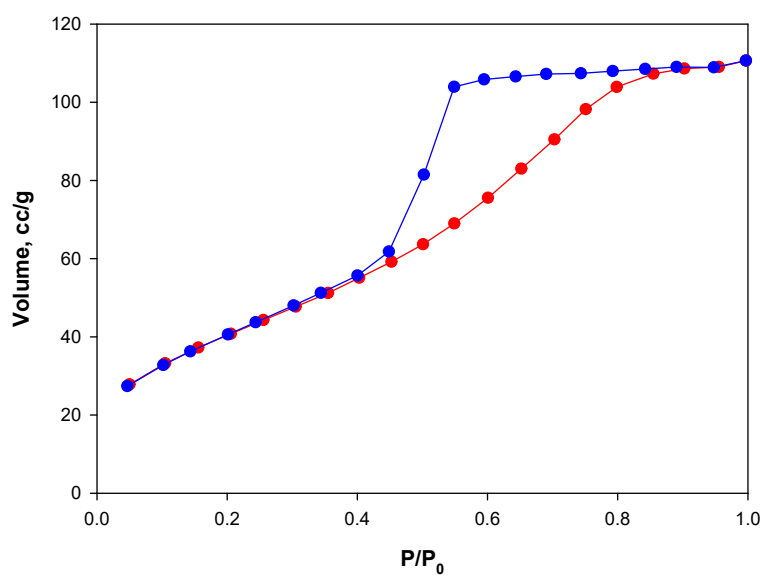


Figure S-6. N₂ adsorption isotherms at 77 K representative of all nanoparticles.

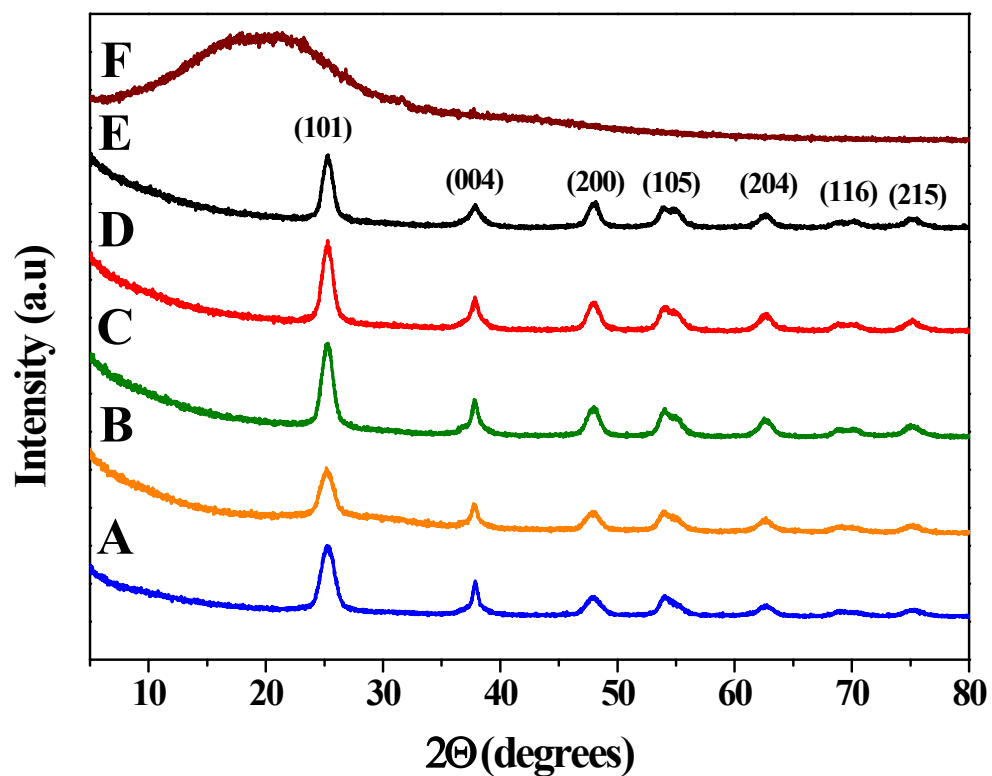


Figure S-7. XRD Spectra of: A) TiO_2 , B) $\text{TiO}_2\text{-DL25}$, C) $\text{TiO}_2\text{-DL50}$, D) $\text{TiO}_2\text{-DL100}$, E) $\text{TiO}_2\text{-DL200}$, F) DL T.

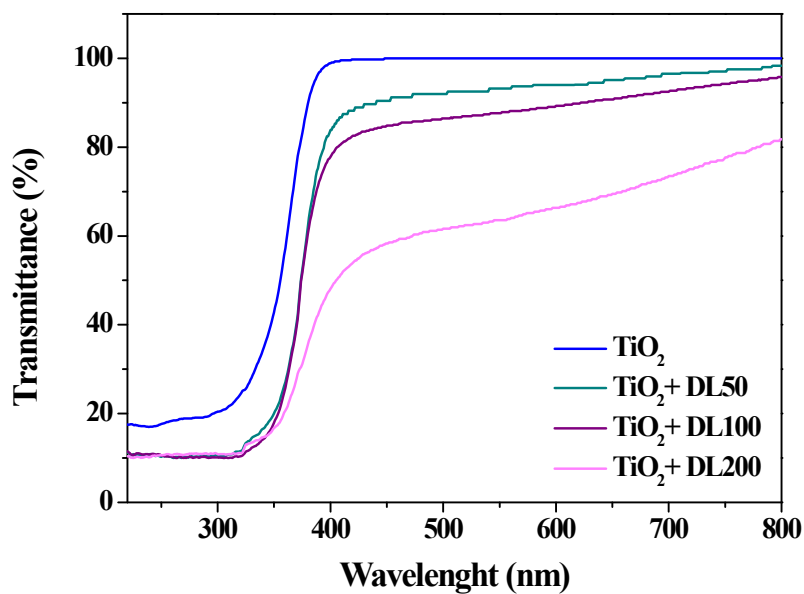


Figure S-8. Transmittance spectra of bare TiO_2 and of physical mixtures of $\text{TiO}_2 + \text{DL50}$, $\text{TiO}_2 + \text{DL100}$ and $\text{TiO}_2 + \text{DL200}$ nanoparticles.

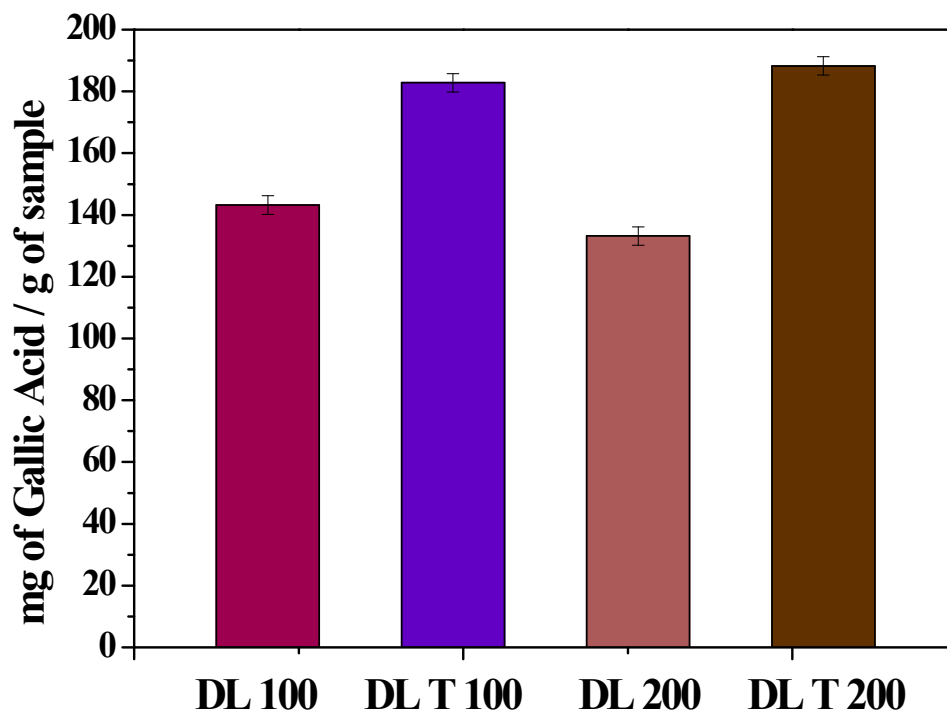


Figure S-9. Total phenolic content of DL100, DL T100, DL200, DL T200 solutions.

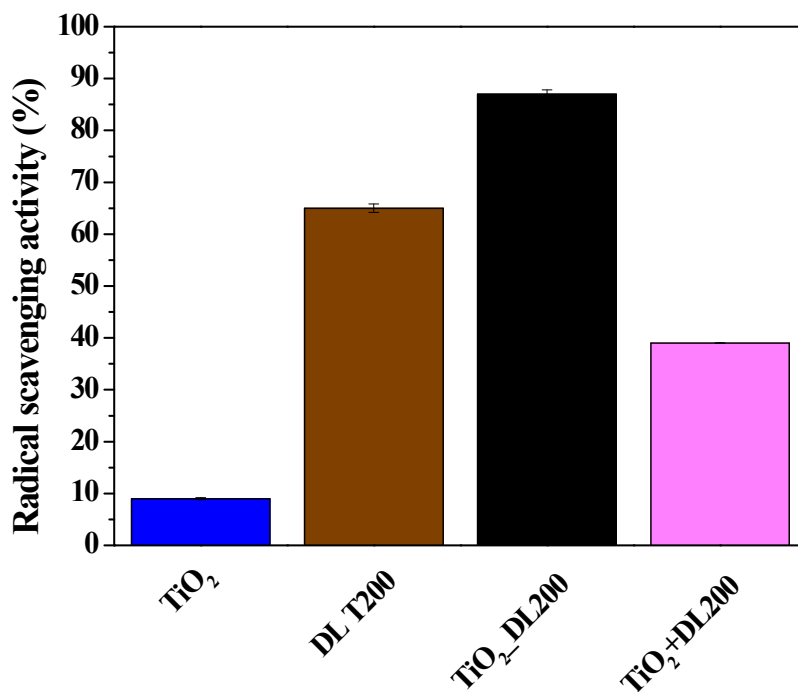


Figure S-10. ABTS radical scavenging activity of TiO₂, DL T200, TiO₂_DL200 and TiO₂ + DL200 samples.

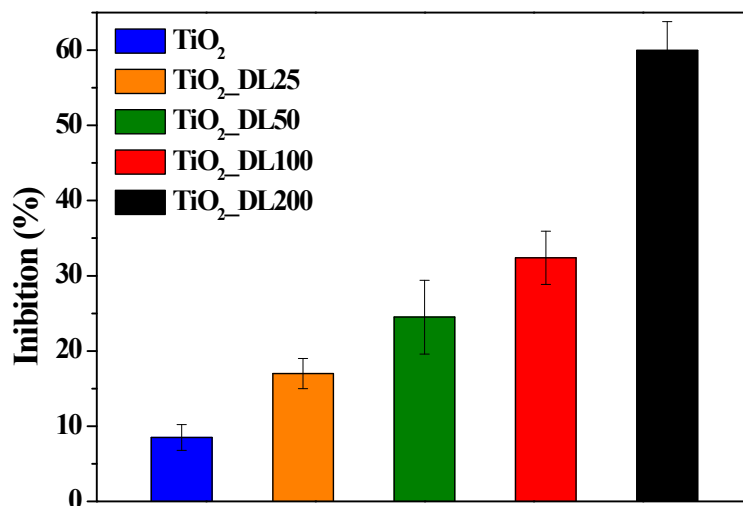


Figure S-11: DPPH analysis on TiO₂, TiO₂_DL100 and TiO₂_DL200 nanomaterials.

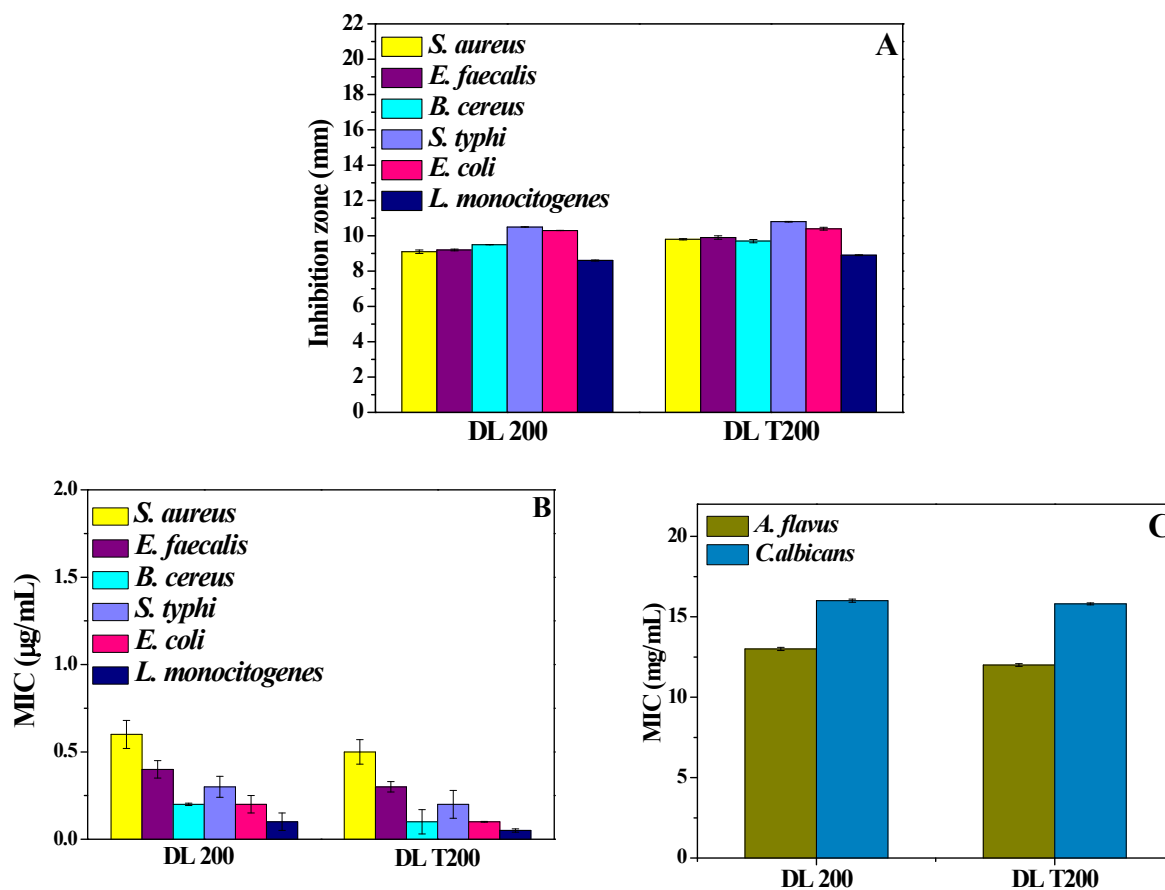


Figure S-12. DDK results (A), MIC against Gram (+) and Gram (-) bacterial (B), MIC against fungi of neat lignin aqueous solution (DL 200) and lignin aqueous solution after the hydrothermal treatment (DL T200) (C).

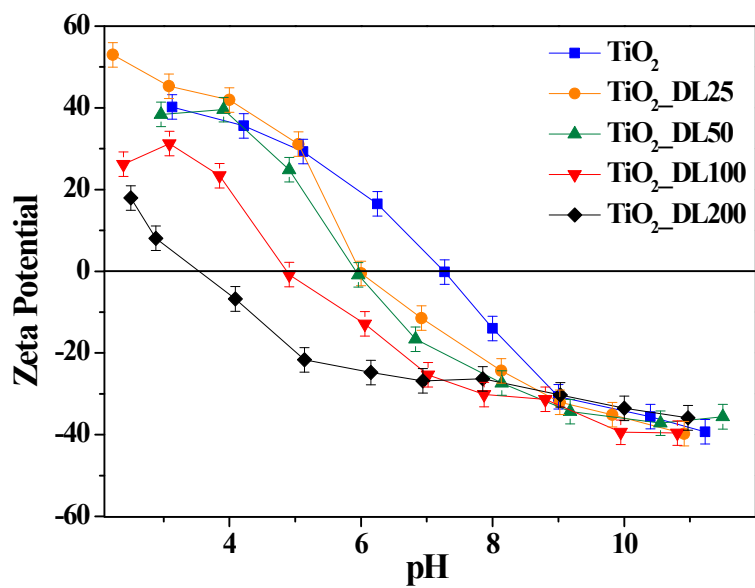


Figure S-13. pH_{zpc} of all nanoparticles.

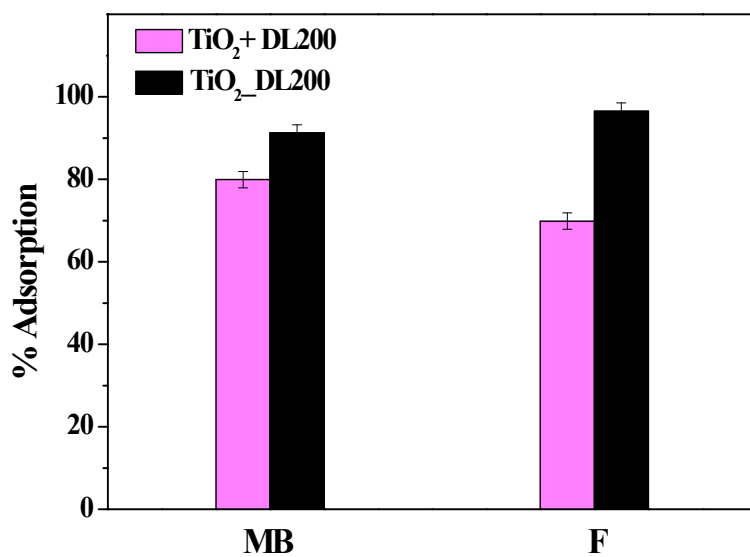


Figure S-14. % MB and % F adsorption capacity of TiO₂-DL200 hybrid nanoparticles and TiO₂ + DL200 physical mixture; $t = 60$ min; $pH = 5.0$; $T = 25$ °C.

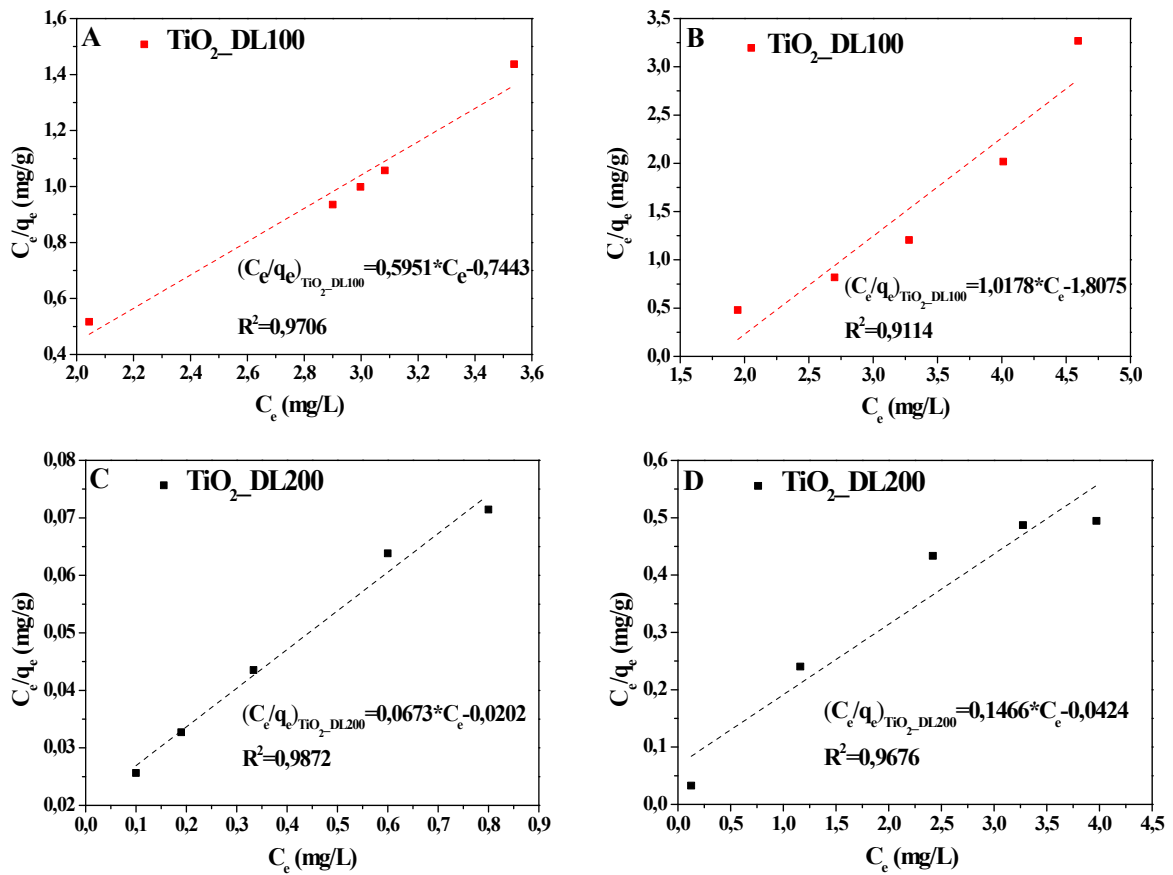


Figure S-15. Langmuir adsorption isotherms for MB (A, C) and F (B, D) dyes in the case of TiO₂_DL100 and TiO₂_DL200 nanoparticles; pH = 5.0; T = 25°C.

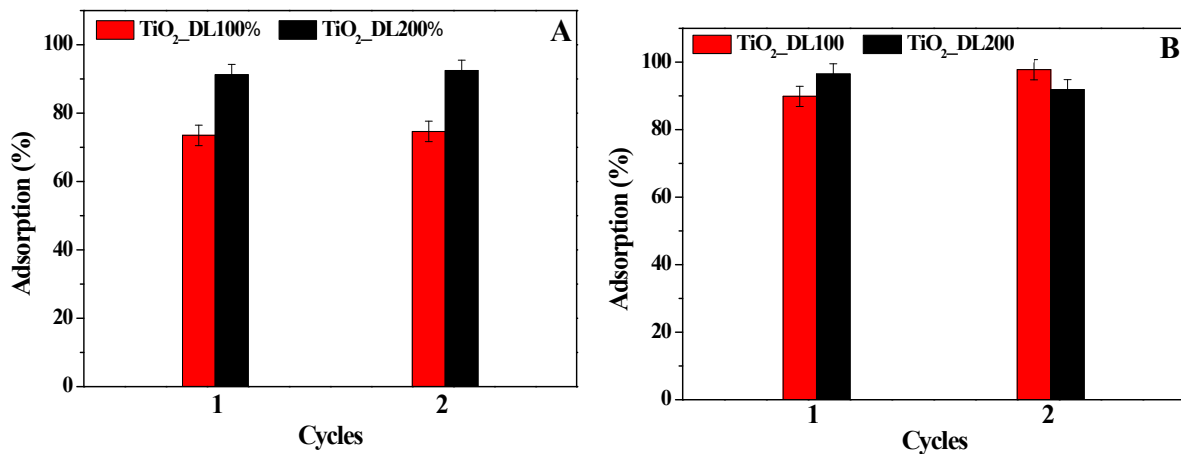


Figure S-16. Operational stability of TiO₂_DL100 and TiO₂_DL200 after two cycles for A) MB and B) F adsorption. t = 60 minutes; pH = 5.0; T = 25 °C.

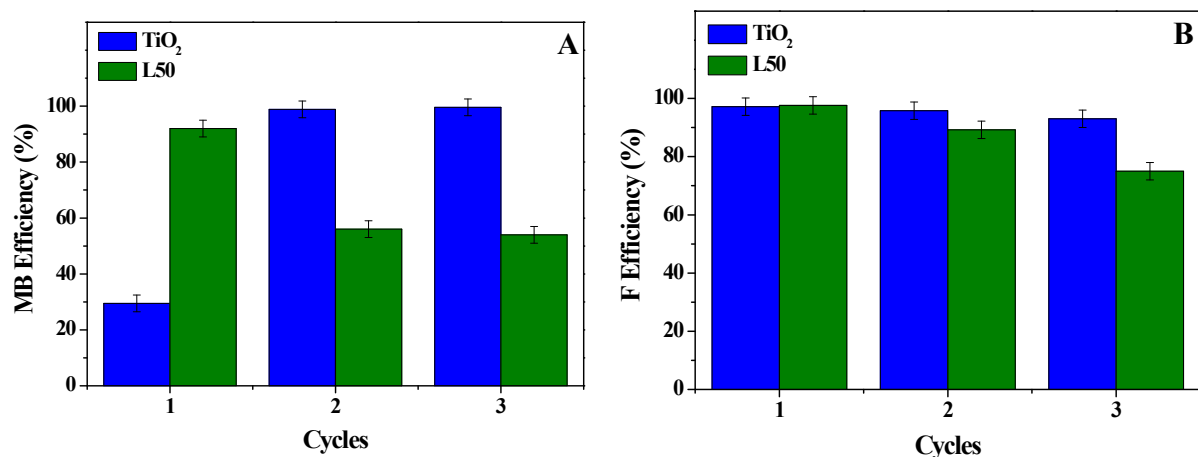


Figure S-17. Operational stability of TiO₂ and TiO₂_DL50 after up to three cycles for A) MB and B) F photocatalytic removal. Reaction time = 120 minutes.

Table S-1: Assignment of FTIR bands of lignin.

Functional group assignment	Wavenumber (cm ⁻¹)
-OH stretching vibration in aromatic and aliphatic hydroxyl groups	3425
C-H asymmetrical and symmetrical vibrations of the methyl (-C ^H ₃)	2940
C-H asymmetrical and symmetrical vibrations of the methylene (-C ^H ₂)	2842
Vibration of aromatic rings	1590, 1510, and 1420
Methoxyl C-H bending	1461
Aromatic C-O stretching of Syringyl units	1350
Aromatic C-O stretching of Guaiacyl units	1265
Phenolic -OH units	1220
Aromatic C-H in plain deformation of the syringyl unit	1128
C-O stretching of secondary alcohol	1084
C-O stretching of primary alcohol	1012
Stretching vibration of aliphatic OH/ether	1030
Aromatic C-H vibration out of plain deformation	852 and 810
Out-of-plane bending of C-OH	620

Table S-2. Hydrodynamic diameters and Zeta potential values of nanoparticles

Sample	Hydrodynamic diameter (D _h) (nm)	Standard deviation	Zeta Potential (mV)	Standard deviation
TiO ₂	165	± 2.9	25	± 2
TiO ₂ _DL25	226	± 4.6	23	± 1

TiO ₂ DL50	236	± 4.3	-1	± 1
TiO ₂ DL100	910	± 1.4	-15	± 1
TiO ₂ DL200	1016	± 4.0	-17	± 2

Table S-3. Mean crystalline size of all nanoparticles.

Sample	Crystalline size (nm)
TiO ₂	≈ 7
TiO ₂ DL25	≈ 7
TiO ₂ DL50	≈ 7
TiO ₂ DL100	≈ 8
TiO ₂ DL200	≈ 12